Supporting Information for

Hydrothermal crystallization of $Ln_2(OH)_4SO_4 \cdot nH_2O$ layered compound for a wide range of Ln (Ln=La-Dy), thermolysis, and facile transformation into oxysulfate and oxysulfide phosphors

Xuejiao Wang,[a,b,c,d] Ji-Guang Li,[a,b,c*] Maxim S. Molokeev,[e,f] Xiaojun Wang,[g] Weigang Liu,[a,b] Qi Zhu,[a,b] Hidehiko Tanaka,[h] Keiko Suzuta,[h] Byung-Nam Kim,[c] and Yoshio Sakka[c]

[a]Key Laboratory for Anisotropy and Texture of Materials (Ministry of Education), Northeastern University, Shenyang, Liaoning 110819, China

[b]Institute of Ceramics and Powder Metallurgy, School of Materials Science and Engineering, Northeastern University, Shenyang, Liaoning 110819, China

[c]Research Centre for Functional Materials, National Institute for Materials Science, Tsukuba, Ibaraki 305-0044, Japan

[d]College of New Energy, Bohai University, Jinzhou, Liaoning 121000, China

[e]Laboratory of Crystal Physics, Kirensky Institute of Physics, Federal Research Center KSC SB RAS, Krasnoyarsk 660036, Russia

[f]Department of Physics, Far Eastern State Transport University, Khabarovsk 680021, Russia

[g]School of Physics and Electronic Engineering, Jiangsu Normal University, Xuzhou, Jiangsu 221116, China

[h]World Premier International Centre for Materials Nanoarchitectonics (WPI-MANA), National Institute for Materials Science, Tsukuba, Ibaraki 305-0044, Japan

[*]Corresponding author

National Institute for Materials Science

Tel: +81-29-860-4394

E-mail: LI.Jiguang@nims.go.jp
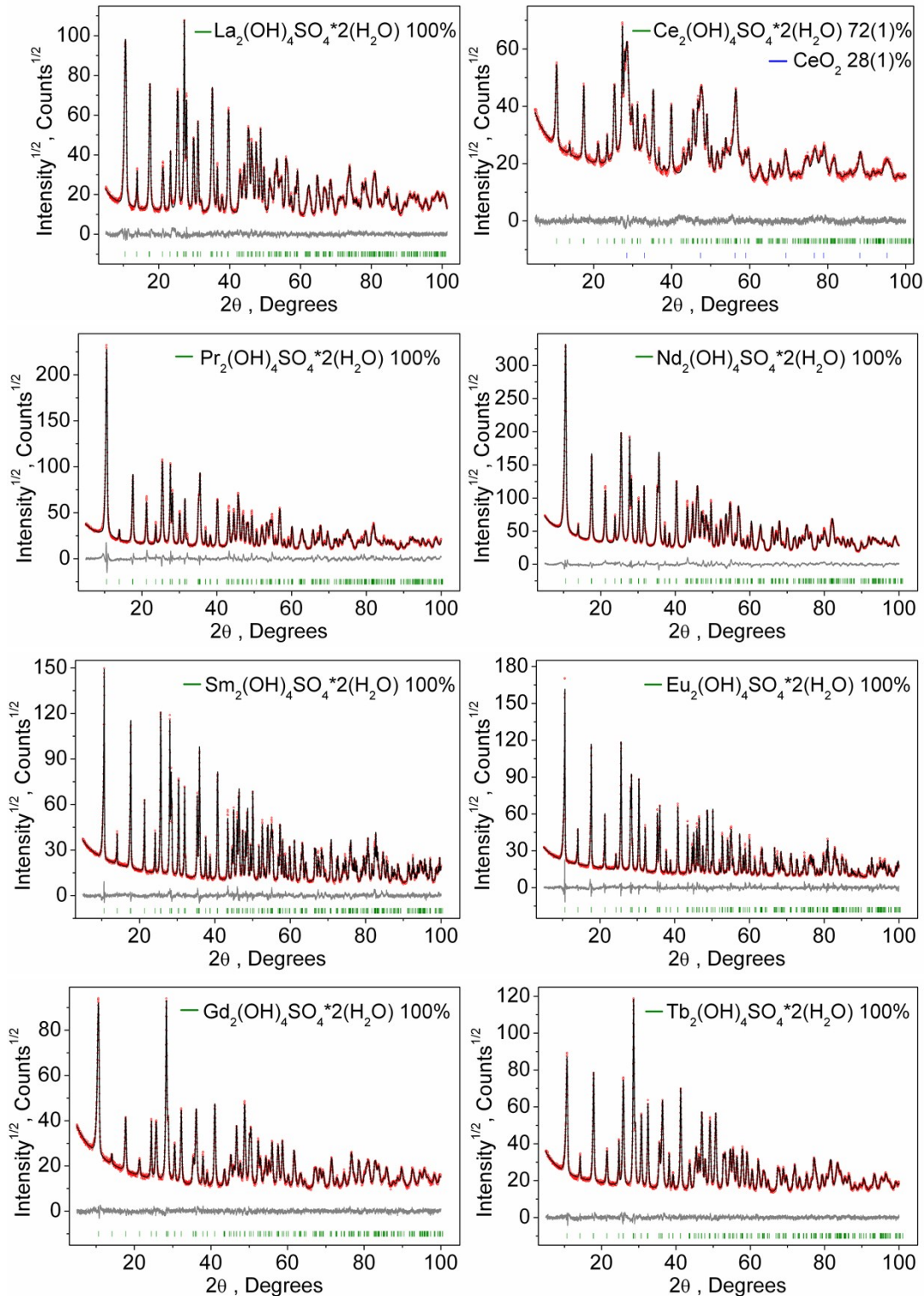
Fig. S1 The observed (black) and calculated (red) XRD profiles and the difference (gray) for $Ln_2(OH)_4SO_4 \cdot nH_2O$ (Ln=La-Tb). The Bragg reflections are indicated with green tick marks.

2

Figure S1 shows the results of Rietveld structure refinements for the sulfate-type layered hydroxides using the crystallographic data of their $La_2(OH)_4SO_4 \cdot nH_2O$ analogue as initial structure model.[1] All the above refinements are stable and give well acceptable reliability factors (Table S2).

Table S1 Results of elemental analysis and the derived chemical formula for the typical compounds hydrothermally obtained at 100 °C and pH=9. Nitrogen and carbon were assumed to solely come from NO_3^- and CO_3^{2-}, respectively, which were assumed to replace OH^-. The amount of OH^- was derived from molecular neutrality, and the water content was calculated with the Ln content.

Results of elemental analysis (wt%)				Chemical formula
Ln	S	N	C	
La 56.9	6.9	0.04	0.16	$La_2(OH)_{3.75}(SO_4)_{1.05}(NO_3)_{0.01}(CO_3)_{0.07} \cdot 2.28H_2O$
Pr 57.4	6.8	0.18	0.22	$Pr_2(OH)_{3.68}(SO_4)_{1.04}(NO_3)_{0.06}(CO_3)_{0.09} \cdot 2.09H_2O$
Eu 60.4	6.5	0.16	0.09	$Eu_2(OH)_{3.85}(SO_4)_{1.02}(NO_3)_{0.05}(CO_3)_{0.03} \cdot 1.70H_2O$
Gd 62.0	5.2	0.26	0.23	$Gd_2(OH)_{4.07}(SO_4)_{0.83}(NO_3)_{0.09}(CO_3)_{0.09} \cdot 1.82H_2O$
Tb 64.0	3.2	0.10	0.12	$Tb_2(OH)_{4.86}(SO_4)_{0.50}(NO_3)_{0.04}(CO_3)_{0.05} \cdot 2.33H_2O$
Ho 64.8	3.3	0.02	0.29	$Ho_2(OH)_{4.71}(SO_4)_{0.52}(NO_3)_{0.01}(CO_3)_{0.12} \cdot 2.24H_2O$
Lu 68.3	3.7	0.06	0.26	$Lu_2(OH)_{4.58}(SO_4)_{0.59}(NO_3)_{0.02}(CO_3)_{0.11} \cdot 1.11H_2O$

Table S2 Main parameters of processing and the reliability factors of refinement for $Ln_2(OH)_4SO_4 \cdot nH_2O$.

Phase	Weight (%)	Sp.gr.	R_{wp}, (%)	R_p,(%)	χ^2	R_B (%)
$La_2(OH)_4SO_4 \cdot nH_2O$	100	$C2/m$	6.43	4.68	1.58	1.47
$Ce_2(OH)_4SO_4 \cdot nH_2O$	72 (1)	$C2/m$	5.51	4.21	1.40	1.55
CeO_2	28 (1)	Fm-$3m$				1.45
$Pr_2(OH)_4SO_4 \cdot nH_2O$	100	$C2/m$	11.65	9.40	3.58	4.00
$Nd_2(OH)_4SO_4 \cdot nH_2O$	100	$C2/m$	6.38	4.82	3.52	2.70
$Sm_2(OH)_4SO_4 \cdot nH_2O$	100	$C2/m$	7.73	5.91	1.99	3.54
$Eu_2(OH)_4SO_4 \cdot nH_2O$	100	$C2/m$	10.47	8.11	2.50	3.77
$Gd_2(OH)_4SO_4 \cdot nH_2O$	100	$C2/m$	5.97	4.53	1.27	1.04
$Tb_2(OH)_4SO_4 \cdot nH_2O$	100	$C2/m$	5.51	4.24	1.46	0.90

$Dy_2(OH)_4SO_4 \cdot nH_2O$	100	*C2/m*	7.47	5.74	1.57	3.19
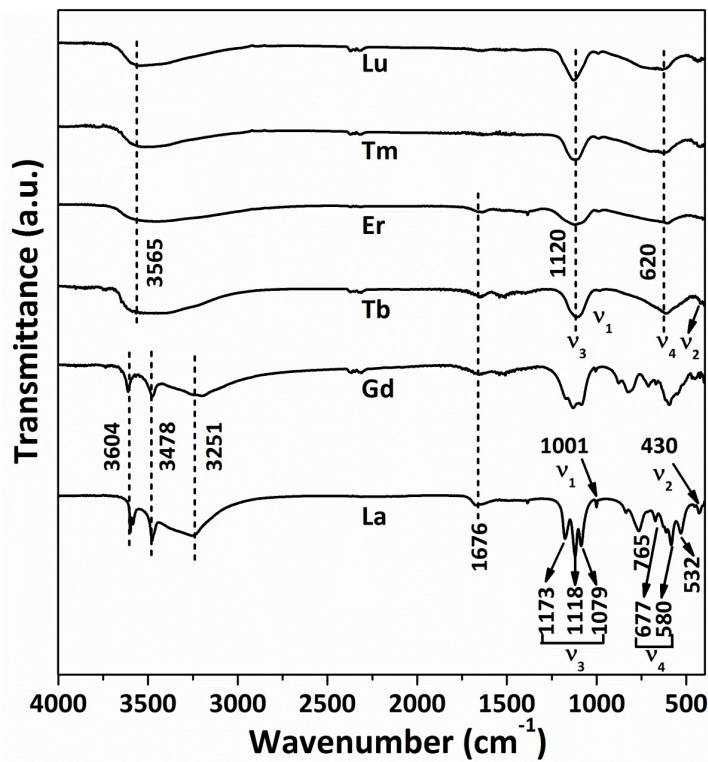
**Fig. S2** FTIR spectra of the typical hydrothermal products synthesized at 100 °C and pH~9.

The La-Gd products show FTIR behaviors similar to the $Ln_2(OH)_4SO_4 \cdot nH_2O$ layered compound as reported before.[1,2] The vibrations at ~3251 and 1676 cm^{-1} can be attributed to the O-H stretching vibrations (v_1 and v_3) and H-O-H bending mode (v_2) of hydration water in the structure, respectively, while the those at ~532 and 765 cm^{-1} are originated from the bending modes of water molecules coordinated to metal ions.[2,3] The two separated sharp bands located at ~3604 and 3478 cm^{-1} can be assigned to hydroxyl (OH$^-$) groups.[3] The fundamental IR vibrations of SO_4^{2-} are documented to be located at ~1104 (v_3), 981 (v_1), 618 (v_4), and 451 cm^{-1} (v_2), and, when the SO_4^{2-} tetrahedron is distorted, the v_3 and v_4 vibrations would split to give rise to two or three peaks with the resolution dependent on the magnitude of the splitting and v_1 and v_2 would become active. The v_1, v_2, v_3, and v_4 fundamental vibrations of sulfate groups were all observed in the La-Gd products as labeled in the figure, with the v_3 and v_4 spilt into several peaks. These indicate that the sulfate groups are directly coordinated to the lanthanide cations

in the structure. Specifically, the v_3 vibration of La-241 show better separated peaks than that of Gd-241, which may indicate that the distortion of SO_4^{2-} in the former is larger than that in the later.[1,4] The Tb-Lu products exhibit similar FTIR behaviors. The absorptions at ~3564 and 1676 cm^{-1} are attributable to the O-H stretching (v_1 and v_3) H-O-H bending (v_2) vibrations of hydration water,[4] respectively. As for the SO_4^{2-} group, the v_3 (1100 cm^{-1}) and v_4 (614 cm^{-1}) bands are non-splitting but with the v_1 (983 cm^{-1}) and v_2 (411 cm^{-1}) vibrations identifiable in the spectra. Such FTIR behaviors may imply that the sulfate ions are not directly coordinated to the lanthanide centres in the hydroxide layers but the tetrahedron of SO_4^{2-} is slightly distorted owing to interaction of the SO_4^{2-} anions with the hydroxyls in the main layer via electrostatic attraction/hydrogen boding. The almost the same FTIR behaviors of the Tm-Lu products and the Tb-Er products further confirm that the four compounds have similar functional groups.
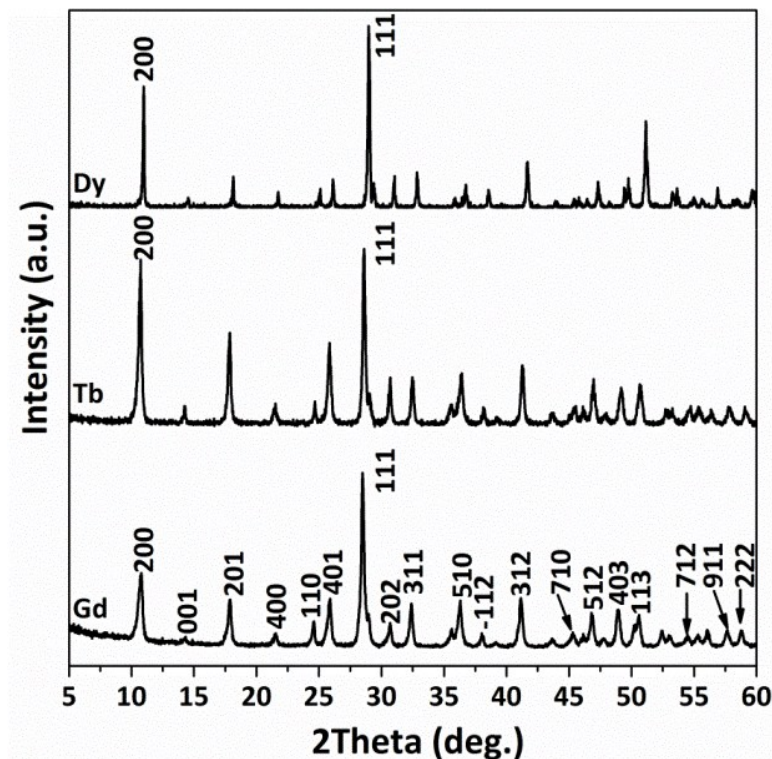

Fig. S3 XRD patterns of the $Ln_2(OH)_4SO_4 \cdot nH_2O$ compounds synthesized at 100 °C and pH=7 (Ln=Gd, Tb, and Dy, as indicted in the figure).
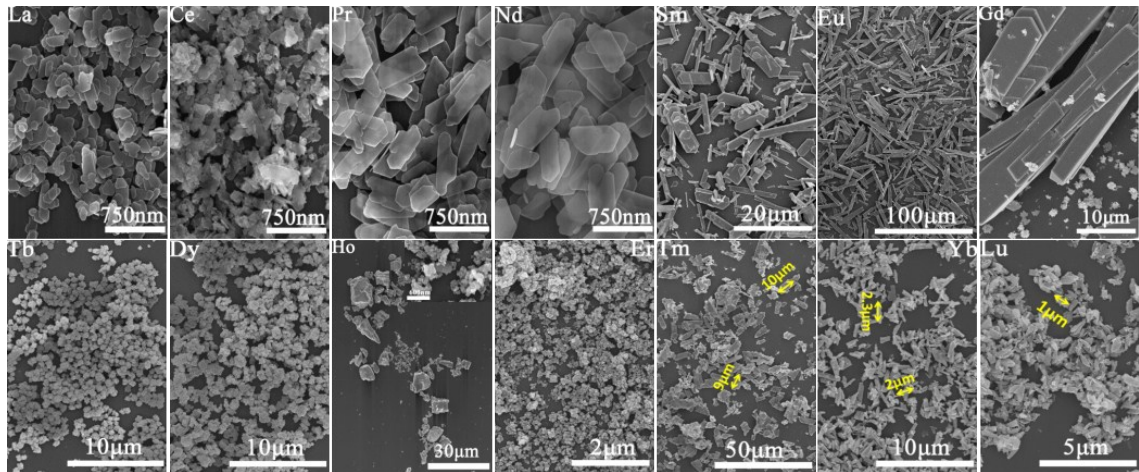
Fig. S4 FE-SEM morphologies of the products hydrothermally synthesized at 100 °C and pH=9.

Table S3 Lattice parameters and axis angle of $Ln_2(OH)_4SO_4 \cdot nH_2O$.

| Sample	a (Å)	b (Å)	c (Å)	β (°)	V (Å³)
$La_2(OH)_4SO_4 \cdot nH_2O$	16.8847 (6)	3.9420 (1)	6.4359 (2)	90.454 (2)	428.36 (3)
$Ce_2(OH)_4SO_4 \cdot nH_2O$	16.8000 (2)	3.8920 (4)	6.3943 (8)	90.445 (5)	418.08 (8)
$Pr_2(OH)_4SO_4 \cdot nH_2O$	16.7590 (2)	3.8572 (5)	6.3570 (9)	90.391 (3)	410.92 (9)
$Nd_2(OH)_4SO_4 \cdot nH_2O$	16.7421 (6)	3.8307 (1)	6.3369 (3)	90.296 (3)	406.40 (3)
$Sm_2(OH)_4SO_4 \cdot nH_2O$	16.6684 (2)	3.7786 (5)	6.2898 (8)	90.208 (9)	396.14 (9)
$Eu_2(OH)_4SO_4 \cdot nH_2O$	16.6441 (3)	3.7522 (9)	6.2704 (1)	90.114 (1)	391.60 (1)
$Gd_2(OH)_4SO_4 \cdot nH_2O$	16.6362 (8)	3.7312 (1)	6.2530 (3)	90.064 (8)	388.14 (3)
$Tb_2(OH)_4SO_4 \cdot nH_2O$	16.5987 (6)	3.7048 (1)	6.2316 (2)	90.091 (5)	383.21 (2)
$Dy_2(OH)_4SO_4 \cdot nH_2O$	16.5817 (4)	3.6821 (6)	6.2144 (1)	90.034 (4)	379.43 (1)
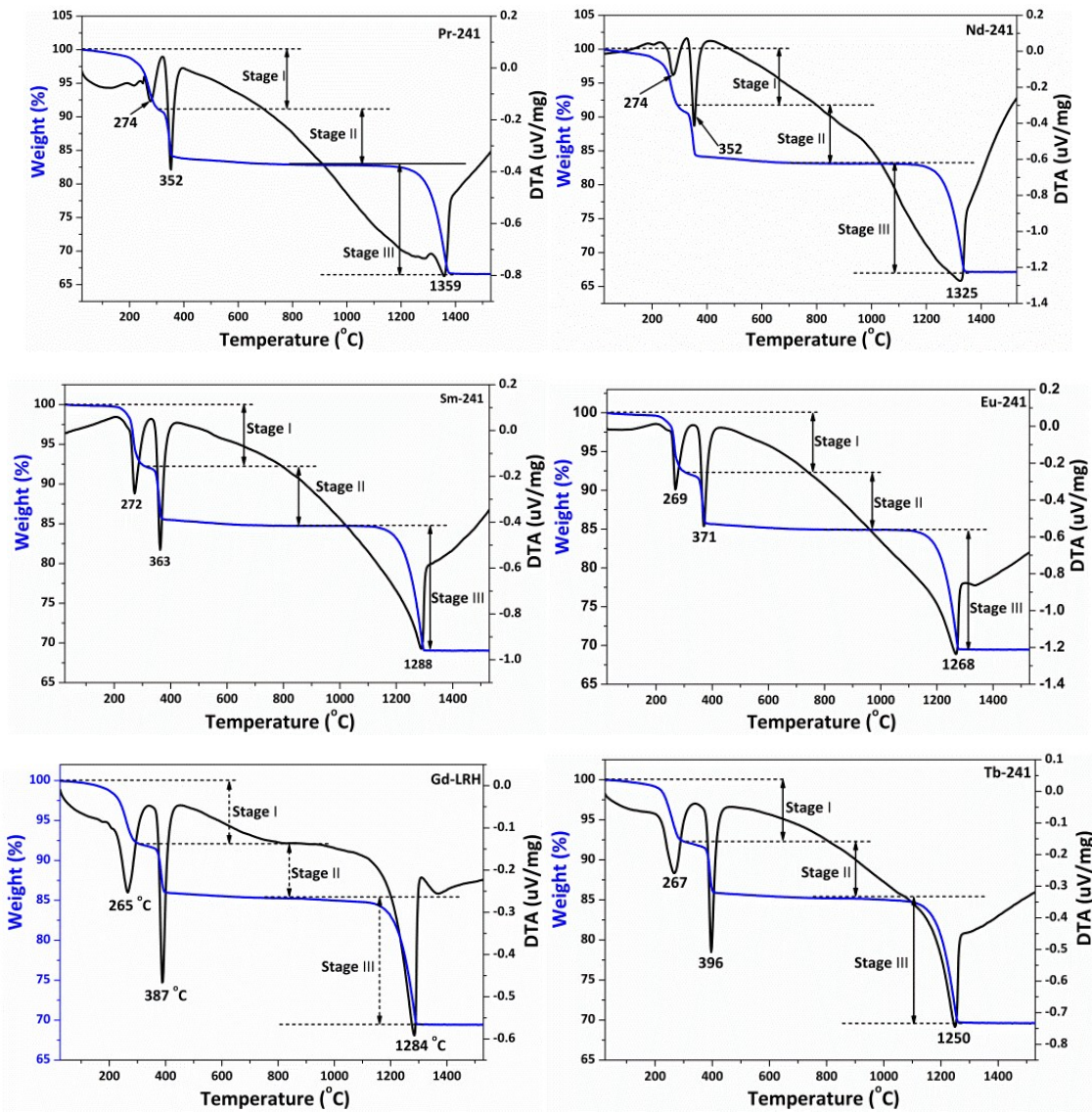
Fig. S5 TG/DTA curves of the Ln-241 compounds (Ln=Pr-Tb, as indicted in the figure).

Table S4 Theoretical weight loss of different stages for the thermal decomposition of $Ln_2(OH)_4SO_4 \cdot nH_2O$ (Ln=La-Dy, except for Ce).

Ln	Molecular weight	Theoretical weight loss of stage II (%)	Theoretical weight loss of stage III (%)	Theoretical total weight loss (%)
La	481.42	7.48	16.62	32.32
Pr	488.50	7.37	16.38	32.48
Nd	494.10	7.29	16.19	31.89
Sm	503.98	7.14	15.87	30.76
Eu	506.88	7.10	15.78	30.56
Gd	516.88	6.96	15.48	29.96
Tb	520.58	6.92	15.37	29.72
Dy	525.48	6.85	15.22	28.99

Table S5 Lattice constants, axis angle and cell volume for the derived $Ln_2O_2SO_4$.

Samples	a (Å)	b (Å)	c (Å)	β (°)	V (Å³)
$La_2O_2SO_4$	14.3521(3)	4.2855(4)	8.3883(1)	493.361(8)	107.01(2)
$Pr_2O_2SO_4$	14.0543(2)	4.2446(2)	8.2835(2)	472.291(6)	107.11(3)
$Nd_2O_2SO_4$	13.9680(5)	4.2253(5)	8.2318(5)	464.267(5)	107.13(4)
$Sm_2O_2SO_4$	13.7495(6)	4.2016(6)	8.1666(6)	450.521(8)	107.27(6)
$Eu_2O_2SO_4$	13.6591(3)	4.1901(2)	8.1355(2)	444.519(3)	107.31(7)
$Gd_2O_2SO_4$	13.6028(4)	4.1793(2)	8.1047(2)	439.816(3)	107.34(3)
$Tb_2O_2SO_4$	13.4850(3)	4.1675(1)	8.0747(3)	433.336(4)	107.27(2)
$Dy_2O_2SO_4$	13.3950(5)	4.1550(3)	8.0478(6)	427.207(1)	107.49(3)
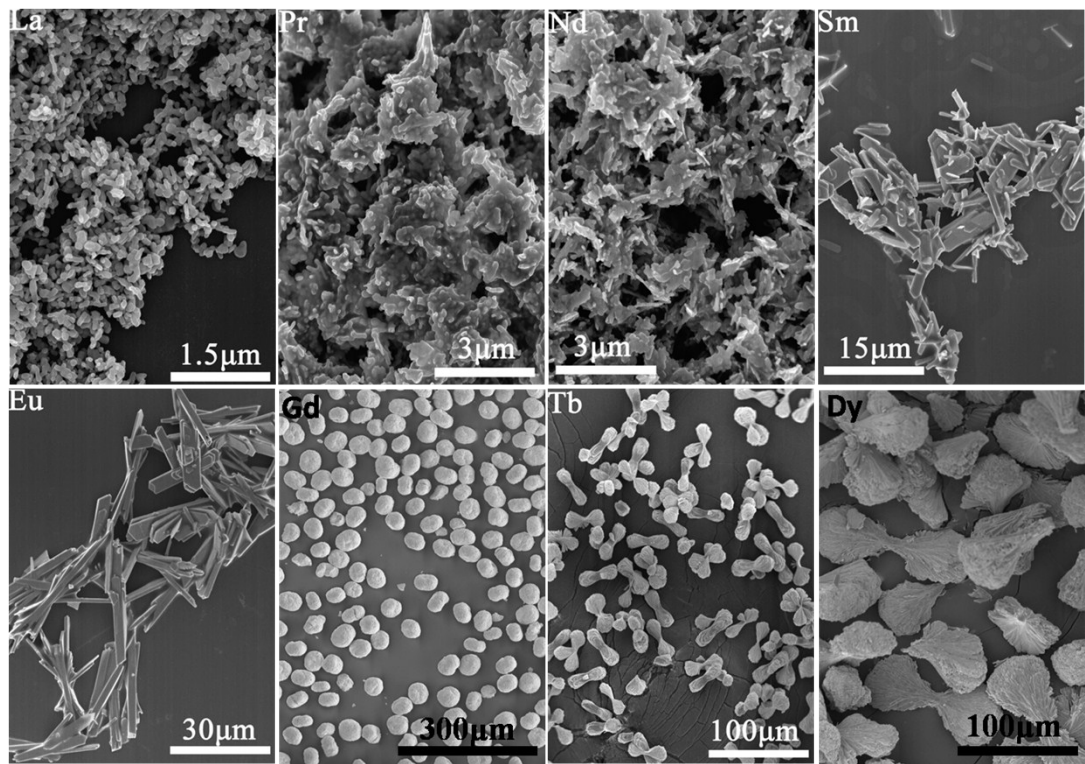
Fig. S6 FE-SEM morphologies of the $Ln_2O_2SO_4$ calcined from $Ln_2(OH)_4SO_4 \cdot nH_2O$ (Ln-241) at 1000 °C for 1 h in the air (in Ar for Tb-241 and Pr-241).

Table S6 Lattice constants, axis angle and cell volume for the derived Ln_2O_2S.

Sample	a (Å)	b (Å)	c (Å)	α (°)	β (°)	γ (°)	V (Å^3)
La_2O_2S	4.0520(2)	4.0520(5)	6.9463(6)	90	90	120	98.77(5)
Pr_2O_2S	3.9682(3)	3.9682(5)	6.7861(4)	90	90	120	92.54(2)
Nd_2O_2S	3.9401(1)	3.9401(8)	6.7525(7)	90	90	120	90.78(9)
Sm_2O_2S	3.8851(5)	3.8851(4)	6.6534(8)	90	90	120	86.97(7)
Eu_2O_2S	3.8695(7)	3.8695(2)	6.6460(7)	90	90	120	86.18(3)
Gd_2O_2S	3.8484(6)	3.8484(8)	6.6406(9)	90	90	120	85.17(4)
Tb_2O_2S	3.8235(5)	3.8235(3)	6.5981(3)	90	90	120	83.53(5)
Dy_2O_2S	3.8016(3)	3.8016(2)	6.5564(7)	90	90	120	82.06(6)
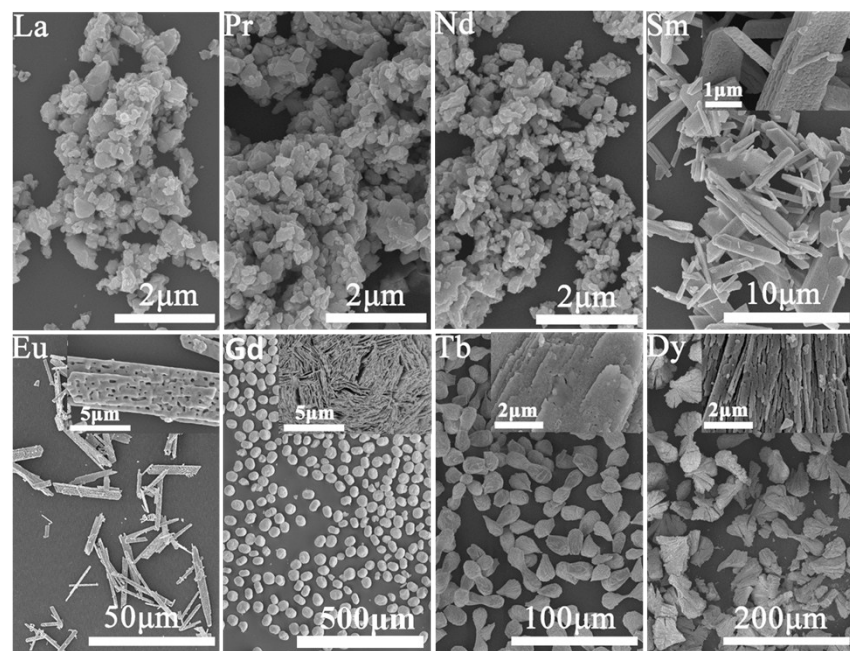
Fig. S7 FE-SEM morphologies of the Ln_2O_2S calcined from $Ln_2(OH)_4SO_4 \cdot nH_2O$ in H_2 at 1200 °C for 1 h (Ln=La-Dy, except for Ce). The insets are high resolution images.
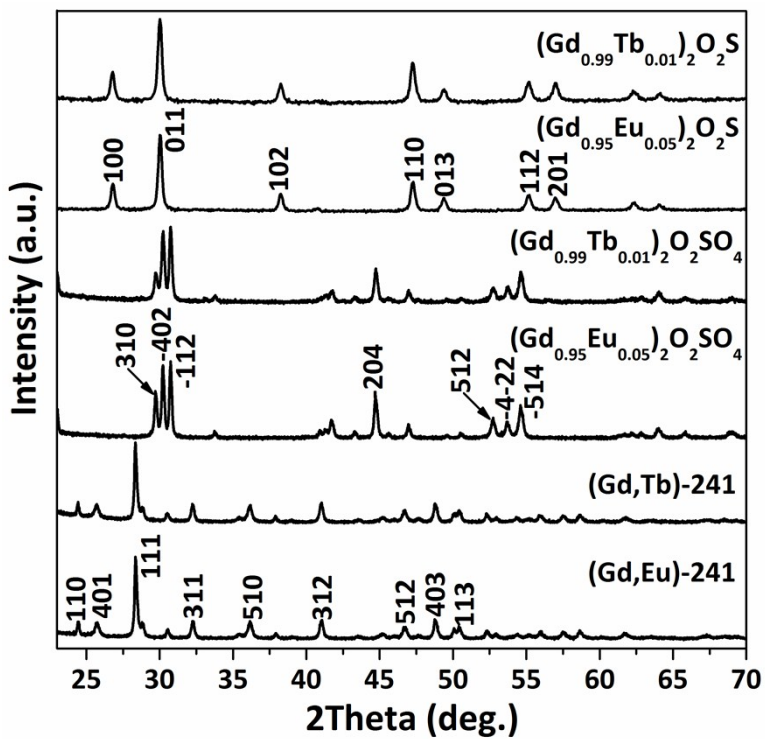
Fig. S8 XRD patterns of $(Gd,RE)_2(OH)_2SO_4 \cdot nH_2O$, $(Gd,RE)_2O_2SO_4$ and $(Gd,RE)_2O_2S$ (RE=5 at% Eu or 1 at% Tb).

Table S7 Structure parameters of $(Gd,RE)_2(OH)_2SO_4 \cdot nH_2O$, $(Gd,RE)_2O_2SO_4$ and $(Gd,RE)_2O_2S$ (RE=5 at% Eu or 1 at% Tb).

Sample	Sp.Gr.	a (Å)	b (Å)	c (Å)	α (°)	β (°)	γ (°)	V (Å^3)
$(Gd_{0.95}Eu_{0.05})$-241	$C2/m$	16.6381(7)	3.7327(3)	6.2582(6)	90	90.266(5)	90	388.66(2)
$(Gd_{0.99}Tb_{0.01})$-241	$C2/m$	16.6127(4)	3.7317(5)	6.2466(8)	90	90.264(7)	90	387.24(3)
$(Gd_{0.95}Eu_{0.05})_2O_2SO_4$	$C2/c$	13.6189(6)	4.1810(8)	8.1312(1)	90	107.439(2)	90	441.71(4)
$(Gd_{0.99}Tb_{0.01})_2O_2SO_4$	$C2/c$	13.5971(3)	4.1770(3)	8.0997(2)	90	107.463(8)	90	438.81(7)
$(Gd_{0.95}Eu_{0.05})_2O_2S$	$P\text{-}3m1$	3.8518(4)	3.8518(8)	6.6686(3)	90	90	120	85.68(6)
$(Gd_{0.99}Tb_{0.01)2}O_2S$	$P\text{-}3m1$	3.8500(7)	3.8500(9)	6.6547(4)	90	90	120	85.42(8)

Smaller lattice constants and cell volume were observed for the Tb^{3+} doped samples, owing to the smaller cation radius of Tb^{3+} (1.095 Å for CN=9) than that of Eu^{3+} (for 1.120 Å for CN=9).[5]
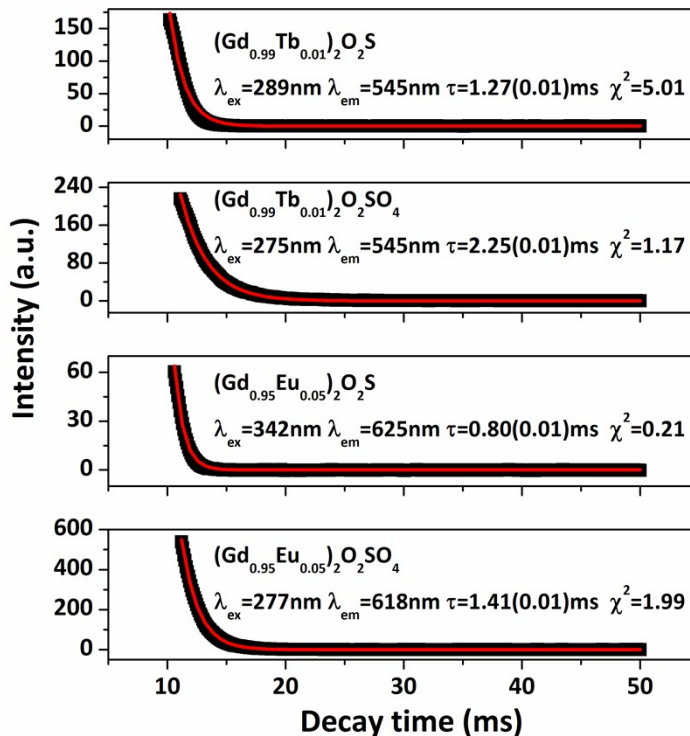

Fig. S9 Fluorescence decay kinetics for the $(Gd,RE)_2O_2SO_4$ and $(Gd,RE)_2O_2S$ phosphors (RE=5 at% Eu or 1 at% Tb). The composition, excitation and emission wavelengths, derived fluorescence lifetime (τ), and the Chi-square (χ^2) factor of single-exponential fitting are indicted in the figure. For the lifetime, the number in bracket represents standard deviation. The experimental data are in black and the results of exponential fitting are in red.
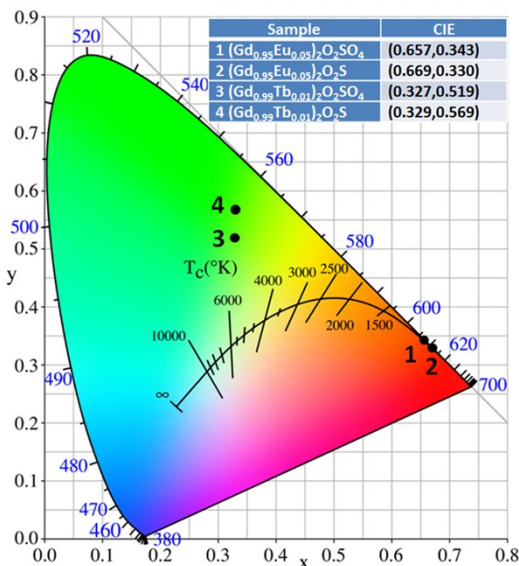
Fig. S10 CIE chromaticity diagram for the emissions of $(Gd,RE)_2O_2SO_4$ and $(Gd,RE)_2O_2S$ (RE=5 at% Eu or 1 at% Tb) phosphors.

The Eu^{3+} and Tb^{3+} doped phosphors emit vivid red and green colors. The color coordinates of $(Gd,Eu)_2O_2SO_4$ and $(Gd,Eu)_2O_2S$ are located on the outer curved boundary in the CIE diagram. The outer boundary is called spectral locus, which corresponds to monochromatic light, and more saturated colors appear closer to the outer curved boundary in the CIE chromaticity diagram.[6,7] Therefore, the emissions of Eu^{3+}-doped $Gd_2O_2SO_4$ and Gd_2O_2S are of good monochromatic lights with high color saturation.

Reference
1. X. J. Wang, J.-G. Li, M. S. Molokeev, et al. *Chem. Eng. J.*, 2016, **302**, 577.
2. J. B. Liang, R. Z. Ma, F. X. Geng, Y. Ebina, T. Sasaki, *Chem. Mater.,* 2010, **22**, 6001.
3. J. A. Gadsden, Infrared spectra of minerals and related inorganic compounds, Butterworth, Newton, MA, 1975.
4. F. X. Geng, R. Z. Ma, Y. Matsushita, J. B. Liang, Y. Michiue, T. Sasaki, *Inorg. Chem.,* 2011, **50**, 6667.
5. R. D. Shannon, *Acta Crystallogr.,* 1976, **A32**, 751.
6. R. L. Booker, *J. Opt. Soc. Am.* 1981, **71**, 139.
7. X.-Z. Huang, Z. Liu, Y. Y. Yang and Y. Tian, *Funct. Mater. Lett.*, 2013, **6**, 1350019.